Taiwanese Journal of Obstetrics & Gynecology 56 (2017) 196–203

Contents lists available at ScienceDirect

Taiwanese Journal of Obstetrics & Gynecology

journal homepage: www.tjog-online.com

Original Article

A promising protein responsible for overactive bladder in ovariectomized mice

Huey-Yi Chen [a, b], Chao-Jung Chen [a, b], Wen-Chi Chen [a, b], Shih-Jing Wang [a], Yung-Hsiang Chen [a, b, c, *]

[a] Graduate Institute of Integrated Medicine, College of Chinese Medicine, Proteomics Core Laboratory, Research Center for Chinese Medicine & Acupuncture, China Medical University, Taichung, Taiwan
[b] Departments of Obstetrics and Gynecology, Medical Research, and Urology, Sex Hormone Research Center, China Medical University Hospital, Taichung, Taiwan
[c] Department of Psychology, College of Medical and Health Science, Asia University, Taichung, Taiwan

ARTICLE INFO

Article history:
Accepted 7 November 2016

Keywords:
estradiol
ovariectomy
overactive bladder
tight junction
urothelium

ABSTRACT

Objective: Ovariectomy (OVX) in mice is a model mimicking a neuro-electronic proof of an overactive bladder in postmenopausal women. Overactive bladder (OAB) was recently found to be due to an altered gap junction protein in a rat model. Thus, this study was conducted to evaluate changes in cell junction protein expression and composition in the bladder of OVX mice.
Materials and Methods: Thirty-six virgin female mice were randomized into three groups: mice with a sham operation only (control), OVX mice without estradiol (E2) replacement, and OVX mice with E2 replacement (OVX + E2). Cystometry assessment was conducted and cell junction-associated protein zonula occludens-2 (ZO-2) expression was measured after 8 weeks. Voiding interval values (time between voids) were assessed in mice under anesthesia. After measurements, the bladders were removed for proteomic analysis using the label-free quantitative proteomics and liquid chromatography–mass spectrometry technology. Lastly, immunohistochemistry (IHC) and Western blot were used to confirm the location and level, respectively, of ZO-2 expression.
Results: We identified 73 differentially expressed proteins in the bladder of OVX mice. The OVX mice showed significantly lower voiding interval values. Voiding interval values were significantly higher in the OVX + E2 group than in the OVX group. Urothelial thicknesses in the bladder were also significantly lower in the OVX group than in the control group. E2 replacement reversed the urothelium layers. Additionally, the expression of ZO-2, a tight junction protein, was the most affected by OVX treatment. IHC and Western blot confirmed the downregulation of ZO-2 in the bladder of OVX mice. Expression of ZO-2 protein was significantly increased in OVX + E2 group compared with OVX group.
Conclusion: This exploratory study estimated changes in protein expression and composition in the bladder of OVX mice. These changes may be associated with the molecular mechanisms of OAB.
© 2017 Taiwan Association of Obstetrics & Gynecology. Publishing services by Elsevier B.V. This is an open access article under the CC BY-NC-ND license (http://creativecommons.org/licenses/by-nc-nd/4.0/).

Introduction

Overactive bladder (OAB) is a common condition affecting elderly people. The prevalence of OAB increases with advancing age, with up to 40% of postmenopausal women being affected [1–3]. According to the recent definition of the International Urogynecological Association and International Continence Society, OAB is a urological disorder defined by bothersome symptoms of urgency with or without urgency urinary incontinence, typically accompanied by frequency and nocturia, in the absence of proven infection or other obvious pathologies [4,5]. With an overall prevalence of around 12% [6], OAB has a significant negative impact on quality of life [7].

There are many theories behind the etiology of OAB, but it is generally accepted that it is caused by a combination of myogenic and neurogenic alterations [8]. It is also believed that mucosal sensory systems also contribute to the disorder [9]. The urothelium, a specialized lining of the urinary tract, functions as an integral part of a sensory web which receives, amplifies, and transmits information regarding its external milieu. Nocchi et al [10] showed that

* Corresponding author. Graduate Institute of Integrated Medicine, China Medical University, Number 91, Hsueh-Shih Road, Taichung 40402, Taiwan.
E-mail address: yhchen@mail.cmu.edu.tw (Y.-H. Chen).

http://dx.doi.org/10.1016/j.tjog.2016.11.006
1028-4559/© 2017 Taiwan Association of Obstetrics & Gynecology. Publishing services by Elsevier B.V. This is an open access article under the CC BY-NC-ND license (http://creativecommons.org/licenses/by-nc-nd/4.0/).

induction of oxidative stress causes functional alterations in mouse urothelium, suggesting possible mechanisms by which oxidative stress causes physiological alterations in the bladder, which may also occur in other organs susceptible to aging [11,12].

Urothelial tight junctions play an important role in the formation of the blood–urine barrier. Tight junctions are essential for normal function of epithelia, restricting paracellular diffusion and contributing to the maintenance of cell surface polarity. Superficial cells of the urothelium develop tight junctions, the basis for the paracellular permeability barrier of the bladder against diffusion of urinary solutes. Rickard et al [13] showed that the tight junctions-associated proteins zonula occludens (ZO-1, ZO-2, and ZO-3) were localized at cell margins. The damage to urothelial tight junctions causes the disruption of barrier function, which induces urinary tract diseases [14]. More recently, ovariectomized rats were found to exhibit frequent bladder contraction and increased connexin-43 expression without changes in muscarinic receptor expression. These results imply that ovariectomy (OVX)-induced OAB may be due to an altered gap junction protein function rather than muscarinic receptor modification [15].

The relative contribution of each of these hypothetical pathways in the development of OAB remains unknown. The bladder and its surrounding structures are rich in estrogen receptors, and physiological and anatomical changes occur around and immediately after menopause [16,17]. After lifestyle changes and bladder retraining, antimuscarinic drugs combined with local estrogens constitute the first-line treatment in postmenopausal women with OAB [18,19]. Although treatments with 17β-estradiol (E2) result in increasing voiding interval, the mechanism of estrogen against OAB is unclear. Due to the limited availability of human tissues, animal models are an important adjunct in improving our understanding of the effects of estrogen on OAB.

Proteomic approaches to identify and quantify the entire protein content of a tissue at a given time may provide insights into disease mechanisms [20]. In this study, we sought to understand the molecular mechanism of OVX-related OAB using label-free quantitative proteomics and nano-liquid chromatography–mass spectrometry (LC-MS/MS) technology. We evaluated changes in protein expression or composition in the bladders of mice treated with and without OVX. This information could offer interesting clues regarding the pathogenesis of OVX-related OAB, and may suggest several avenues for novel research and potential new therapies.

Materials and methods

OVX-induced OAB model in mice

Thirty-six virgin female C57BL/6 mice, aged 6–8 weeks, were randomized into three groups (n = 12, respectively): Group 1—mice with sham operation only (control), Group 2—OVX mice without estradiol (E2) replacement [placebo with vehicle (250 μL subcutaneously; 10% dimethyl sulfoxide, 90% corn oil; Sigma-Aldrich, St. Louis, MO, USA)], and Group 3—OVX mice with E2 replacement (5 μg/kg subcutaneously; Sigma-Aldrich). Four weeks after OVX, mice received either E2 or placebo for 4 weeks. The mice undergoing OVX or sham operation were anesthetized with 1.5% isoflurane. In Group 1, midline longitudinal abdominal incision was excised and then closed with 2-0 silk. In Groups 2 and 3, both ovaries were excised through midline longitudinal abdominal incision that was then closed with 2-0 silk [21]. In the pilot experiments, the time at which the maximum effect on OAB was observed was after Day 56 (8 weeks). The experiments were performed on the 8th week after OAB or sham operation. All experimental protocols were approved by the Institutional Animal Care and Use Committee of China Medical University (Reference number: 104-43-N).

Cystometry assessment

The surgical procedure was carried out under urethane (1 g/kg, intraperitoneal, Sigma-Aldrich) anesthesia according to the methods as previously described [22–25]. A suprapubic tube (SPT) implantation (PE-10 tubing, Clay Adams, Parsippany, NJ, USA) was implanted in the bladder. Key points of the operation include: (1) a midline longitudinal abdominal incision was made, 0.5 cm above the urethral meatus; (2) a small incision was made in the bladder wall, and PE-10 tubing with a flared tip was implanted in the bladder dome; and (3) the purse-string suture of 8-0 silk was tightened around the catheter, which was tunneled subcutaneously to the neck, where it exited the skin.

The bladder catheter was connected to both a syringe pump and a pressure transducer. Pressure and force transducer signals were amplified and digitized for computer data collection at 10 samples per second (PowerLabs, ADInstruments, Bella Vista, Australia). The mice were placed supine at the level of zero pressure while bladders were filled with room temperature saline at 20 μL/min through the bladder catheter. After a 30-minute equilibration period, intravesical pressure was recorded for 30 minutes. Voiding interval refers to the time between voids is measured from the start of a voiding contraction to the start of the next [26].

After confirmation with cystometry, the mice were sacrificed, and the bladders were removed for proteomics, Western blot analyses (n = 6 for each group), and for histological examination, immunohistochemistry (IHC) staining (n = 6 for each group), respectively.

Protein preparation

Frozen tissue sample were pulverized with a liquid nitrogen-chilled mortar and pestle. Tissue powder was then homogenized in buffer (16 mM potassium phosphate, pH 7.8, 0.12 mol/L NaCl, 1 mM ethylene diamine tetra-acetic acid, Sigma-Aldrich) containing a protease inhibitor cocktail (Complete Mini, Roche Diagnostics, Berlin, Germany), and then centrifuged at 10,000g. The supernatant was removed, and the previous homogenization step was repeated after resuspending the remaining tissue pellet in basic buffer. After removal of the second supernatant, the remaining tissue pellet was suspended in urea buffer (6M, Sigma-Aldrich). The samples were centrifuged (13,000g for 30 minutes), and the supernatant was removed. Protein concentration was determined using bicinchoninic acid protein assay (Pierce, Rockford, IL, USA) [27].

Protein identification and label free quantitative proteomics by nanoLC-MS/MS analysis

The nanoLC-MS/MS was performed with a nanoflow UPLC system (UltiMate 3000 RSLCnano system, Dionex, Amsterdam, The Netherlands) coupled with a captive spray ion source and hybrid Quadrupole Time-of-Flight mass spectrometer (maXis impact, Bruker, San Antonio, TX, USA). The sample was injected into a tunnel-frit trap column [C18, 5 μm, 100 Å, packed length of 2 cm, 375 μm outer diameter (od) × 180 μm inner diameter (id)] with a flow rate of 8 μL/min and a duration of 5 minutes. The trapped analytes were separated by a commercial analytical column (Acclaim PepMap C18, 2 μm 100 Å, 75 μm × 250 mm, Thermo Scientific, Waltham, MA, USA) with a flow rate of 300 nL/min. An acetonitrile/water gradient of 1–40% within 90 minutes was used for peptide separation. For MS/MS detection, peptides with charge 2^+, 3^+, or 4^+ and the intensity >20 counts were selected for data

dependent acquisition, which was set to one full MS scan (400–2000 m/z) with 1 Hz and switched to 10 product ion scans (100–2000 m/z) with 10 Hz.

The LC-MS/MS spectra were deisotoped, centroided, and converted to XML files using DataAnalysis (version 4.1, Bruker). The XML files were searched against the Swissport (release 51.0) database using the MASCOT search algorithm (version 2.2.07). The search parameters for MASCOT for peptide and MS/MS mass tolerance were 50 ppm and 0.07 Da, respectively. Search parameters were selected as Taxonomy – mus; enzyme – trypsin; fixed modifications – carbamidomethyl (C); variable modifications – oxidation (M). Peptides were considered as identified if their MASCOT individual ion score was >25 ($p < 0.01$).

Label free quantitative proteomics was achieved by LC-MS replicated runs ($n = 4$) of different groups (6 pooled bladder protein extracts in each group). After LC-MS runs finished, LC-MS/MS runs of each group were performed for protein identification. LC-MS results were processed to have molecular features with DataAnalysis 4.1 (Bruker Daltonics, Bremen, Germany), which were then loaded into ProfileAnalysis software 2.0 (Bruker Daltonics) for *t* test comparison between two groups. The *t* test results among different groups were further transferred to ProteinScape 3.0 (Bruker Daltonics) and combined with protein identification results of each group for the integration of quantified peptide information into each protein [28].

Histological examination

The mice were sacrificed immediately after completing cystometry, and the bladders were harvested. The tissue samples were fixed in 10% buffered formalin (pH 7.4, Sigma-Aldrich) and used for hematoxylin and eosin (H&E) stain (Sigma-Aldrich). Cross sections of the specimens ($n = 6$ for each group) were examined using light microscopy and photographed. The mean thickness of the four regions of the urothelium near the two diagonal lines in the transverse sections of the midbladder was evaluated using Image-Pro Plus 5.1 image analysis software (Silver Spring, Montgomery, MD, USA) [25].

Immunohistochemistry staining

The tissue samples were fixed in 10% buffered formalin, and 10-μm sections were cut. The sections were treated in methanol containing 0.3% hydrogen peroxide (Sigma-Aldrich) for 30 minutes to eliminate endogenous perioxidase activity and washed in phosphate-buffered saline (PBS, Sigma-Aldrich). The sections were then incubated with rabbit anti-ZO-2 primary antibody (1:100 in room temperature for 1 hour, NBP1-86850, Novus Biologicals, Littleton, CO, USA). After being washed with PBS three times, the sections were incubated with a biotinylated secondary antibody. The sections were washed in PBS and then incubated with an avidin–biotin–peroxidase complex (Zymed, South San Francisco, CA, USA) for 30 minutes. After washing with PBS, a chromogenic reaction was developed by incubating with 3,3′-diaminobenzidine tetrahydrochloride substrate kit (Invitrogen, Carlsbad, CA, USA) for 1 minutes, then incubated with Mayer's hematoxylin for 3 minutes. After washing with normal saline for 10 minutes, the sections were viewed under microscopy [22].

Western blot analysis

Protein samples are resolved by appropriate percentage of polyacrylamide gel electrophoresis. Subsequently, proteins in the gel are transferred onto the polyvinylidene difluoride (PVDF, Sigma-Aldrich) membrane with a semidry transfer unit. The PVDF blots are blocked in Tris-buffered saline and Tween 20 containing 2% nonfat dry milk (Sigma-Aldrich), incubated with rabbit anti-ZO-2 primary antibody (1:500 at room temperature for 1 hour, NBP1-86850, Novus Biologicals), followed by a secondary antibody conjugated with horseradish peroxidase. Antibody against glyceraldehyde 3-phosphate dehydrogenase (GAPDH) (1:2,000 at room temperature for 1 hour, NB300-221, Novus Biologicals) was used as loading controls [29]; in the proteomic and pilot studies, we confirmed this protein expression does not change between control and CYP groups. Proteins of interest are visualized with an ECL system (GE Healthcare Bio-Sciences, Pittsburgh, PA, USA) [21].

Statistical analyses

The fold changes of the target tissues are compared by Student *t* test or analysis of variance. All statistical tests were two-sided. A *p*-value < 0.05 was considered statistically significant. All calculations were performed using SPSS (SPSS for Windows, version 8.0, SPSS Inc., Chicago, IL, USA).

Results

Proteomic analysis

A total of 493 proteins were detected, and 365 proteins of them were identified with quantification information. There are 20% (73/365) proteins with significant fold changes. We found 73 differentially expressed proteins between OVX-treated and control female mice; 33 proteins were downregulated and 40 were upregulated (Table 1). Protein identified score, peptide numbers for identification, coefficient of variation (CV) (%) of protein quantification, and peptide numbers for quantification are shown in Table 1. As most proteins were identified and quantified with one peptide, which do not have CV%, possibly due to their less abundance in tissue; these protein ratios could be reliable.

In terms of Gene Ontology database, the differentially expressed proteins of bladder from OVX mice were divided into biological process. Most of the identified OVX-modulated proteins in bladders are involved in cytoskeleton, muscle contraction, cell adhesion, development, signal transduction, and immune response (Table 2). One of the major proteins downregulated by OVX, zonula occludens-2 (ZO-2), is a tight junction (cell-cell adhesion) protein.

Decreased voiding interval values in OVX-treated mice

Fig. 1 shows the cystometry traces and bladder weights between control, OVX-induced OAB, and OVX + E2 group in female mice. Voiding interval values were significantly lower in the OVX group than in the control group. By contrast, voiding interval values were significantly increased ($p < 0.05$) in the OVX + E2 group than in the OVX group (Fig. 1A and B). Bladder weight in the OVX group did not significantly change after OVX or OVX with E2 supplementation (Fig. 1C).

Urothelial thickness and ZO-2 expression in the bladder of OVX-treated mice

Histological examination in bladder by H&E stain between control, OVX-induced OAB, and OVX + E2 group in female mice is shown in Fig. 2. Urothelial thickness in the bladder was significantly lower ($p < 0.05$) in the OVX group than in the control group. By contrast, urothelial thickness in the bladder was significantly increased ($p < 0.05$) in the OVX + E2 group than in the OVX group.

As shown in Table 1, the expression of ZO-2 was affected the most by OVX. Thus, the bladders were histologically examined with

Table 1
Differentially expressed proteins of bladder from female mice with and without OVX.[a]

Accession	Protein	Identified numbers	Scores	OVX/ Control	Quantified peptides	CV (%)
DPYL3_MOUSE	Dihydropyrimidinase-related protein 3 OS = Mus musculus GN = Dpysl3 PE = 1 SV = 1	1	61.5 (M:61.5)	0.03	1	
BRWD1_MOUSE	Bromodomain and WD repeat-containing protein 1 OS = Mus musculus GN = Brwd1 PE = 1 SV = 2	1	32.9 (M:32.9)	0.03	1	
K22 E_MOUSE	Keratin, Type II cytoskeletal 2 epidermal OS = Mus musculus GN = Krt2 PE = 1 SV = 1	5	224.2 (M:224.2)	0.13	1	
ZO2_MOUSE	Tight junction protein ZO-2 OS = Mus musculus GN = Tjp2 PE = 1 SV = 2	1	28.0 (M:28.0)	0.16	1	
RS3_MOUSE	40S ribosomal protein S3 OS = Mus musculus GN = Rps3 PE = 1 SV = 1	2	102.2 (M:102.2)	0.21	1	
KCRU_MOUSE	Creatine kinase U-type, mitochondrial OS = Mus musculus GN = Ckmt1 PE = 1 SV = 1	1	57.9 (M:57.9)	0.23	1	
F192 A_MOUSE	Protein FAM192 A OS = Mus musculus GN = Fam192a PE = 2 SV = 1	1	26.7 (M:26.7)	0.3	1	
HPT_MOUSE	Haptoglobin OS = Mus musculus GN = Hp PE = 1 SV = 1	7	326.6 (M:326.6)	0.4	3	26.34
DX39 B_MOUSE	Spliceosome RNA helicase Ddx39 b OS = Mus musculus GN = Ddx39 b PE = 1 SV = 1	1	37.8 (M:37.8)	0.43	1	
RADI_MOUSE	Radixin OS = Mus musculus GN = Rdx PE = 1 SV = 3	6	300.6 (M:300.6)	0.46	5	240.91
KDM3A_MOUSE	Lysine-specific demethylase 3A OS = Mus musculus GN = Kdm3a PE = 1 SV = 1	1	45.1 (M:45.1)	0.49	1	
NDUA4_MOUSE	NADH dehydrogenase [ubiquinone] 1 alpha subcomplex subunit 4 OS = Mus musculus GN = Ndufa4 PE = 1 SV = 2	2	70.4 (M:70.4)	0.49	1	
IGHM_MOUSE	Ig mu chain C region secreted form OS = Mus musculus GN = Igh-6 PE = 1 SV = 2	4	207.7 (M:207.7)	0.5	1	
TALDO_MOUSE	Transaldolase OS = Mus musculus GN = Taldo1 PE = 1 SV = 2	3	122.0 (M:122.0)	0.5	2	137.53
MOES_MOUSE	Moesin OS = Mus musculus GN = Msn PE = 1 SV = 3	8	367.3 (M:367.3)	0.51	6	205.66
ASAP2_MOUSE	Arf-GAP with SH3 domain, ANK repeat and PH domain-containing protein 2 OS = Mus musculus GN = Asap2 PE = 1 SV = 3	1	33.4 (M:33.4)	0.52	1	
PDIA6_MOUSE	Protein disulfide-isomerase A6 OS = Mus musculus GN = Pdia6 PE = 1 SV = 3	1	46.4 (M:46.4)	0.53	1	
ALDOC_MOUSE	Fructose-bisphosphate aldolase C OS = Mus musculus GN = Aldoc PE = 1 SV = 4	2	141.8 (M:141.8)	0.53	1	
RS5_MOUSE	40S ribosomal protein S5 OS = Mus musculus GN = Rps5 PE = 2 SV = 3	2	52.9 (M:52.9)	0.53	1	
FIBB_MOUSE	Fibrinogen beta chain OS = Mus musculus GN = Fgb PE = 2 SV = 1	2	117.9 (M:117.9)	0.54	1	
SODM_MOUSE	Superoxide dismutase [Mn], mitochondrial OS = Mus musculus GN = Sod2 PE = 1 SV = 3	2	75.9 (M:75.9)	0.55	1	
MYLK4_MOUSE	Myosin light chain kinase family member 4 OS = Mus musculus GN = Mylk4 PE = 2 SV = 2	1	30.2 (M:30.2)	0.58	1	
ALDH2_MOUSE	Aldehyde dehydrogenase, mitochondrial OS = Mus musculus GN = Aldh2 PE = 1 SV = 1	11	666.8 (M:666.8)	0.59	4	24.1
QCR1_MOUSE	Cytochrome b-c1 complex subunit 1, mitochondrial OS = Mus musculus GN = Uqcrc1 PE = 1 SV = 2	1	57.5 (M:57.5)	0.59	1	
MAOX_MOUSE	NADP-dependent malic enzyme OS = Mus musculus GN = Me1 PE = 1 SV = 2	3	167.1 (M:167.1)	0.59	1	
MYL9_MOUSE	Myosin regulatory light polypeptide 9 OS = Mus musculus GN = Myl9 PE = 1 SV = 3	12	849.5 (M:849.5)	0.59	11	36.67
UGDH_MOUSE	UDP-glucose 6-dehydrogenase OS = Mus musculus GN = Ugdh PE = 1 SV = 1	4	290.7 (M:290.7)	0.59	1	
ACADL_MOUSE	Long-chain specific acyl-CoA dehydrogenase, mitochondrial OS = Mus musculus GN = Acadl PE = 2 SV = 2	3	162.2 (M:162.2)	0.59	1	
PSA2_MOUSE	Proteasome subunit alpha type-2 OS = Mus musculus GN = Psma2 PE = 1 SV = 3	1	26.2 (M:26.2)	0.6	1	
TPM1_MOUSE	Tropomyosin alpha-1 chain OS = Mus musculus GN = Tpm1 PE = 1 SV = 1	13	798.0 (M:798.0)	0.61	8	12.04
INMT_MOUSE	Indolethylamine N-methyltransferase OS = Mus musculus GN = Inmt PE = 1 SV = 1	2	89.3 (M:89.3)	0.61	2	0.34
KCRM_MOUSE	Creatine kinase M-type OS = Mus musculus GN = Ckm PE = 1 SV = 1	10	570.2 (M:570.2)	0.61	7	9.82
PPIA_MOUSE	Peptidyl-prolyl cis-trans isomerase A OS = Mus musculus GN = Ppia PE = 1 SV = 2	6	322.2 (M:322.2)	0.61	6	56.5
TCPB_MOUSE	T-complex protein 1 subunit beta OS = Mus musculus GN = Cct2 PE = 1 SV = 4	1	41.6 (M:41.6)	1.5	1	
EHD4_MOUSE	EH domain-containing protein 4 OS = Mus musculus GN = Ehd4 PE = 1 SV = 1	4	213.3 (M:213.3)	1.54	2	17.11
K1C18_MOUSE	Keratin, type I cytoskeletal 18 OS = Mus musculus GN = Krt18 PE = 1 SV = 5	7	253.0 (M:253.0)	1.54	6	19.43
CH60_MOUSE	60 kDa heat shock protein, mitochondrial OS = Mus musculus GN = Hspd1 PE = 1 SV = 1	4	182.3 (M:182.3)	1.58	3	18.63
CAP1_MOUSE	Adenylyl cyclase-associated protein 1 OS = Mus musculus GN = Cap1 PE = 1 SV = 4	5	326.3 (M:326.3)	1.65	4	73.54
RHOA_MOUSE	Transforming protein RhoA OS = Mus musculus GN = Rhoa PE = 1 SV = 1	4	176.5 (M:176.5)	1.72	3	23.46
ARF5_MOUSE	ADP-ribosylation factor 5 OS = Mus musculus GN = Arf5 PE = 2 SV = 2	3	184.9 (M:184.9)	1.75	2	51.73
LUM_MOUSE	Lumican OS = Mus musculus GN = Lum PE = 1 SV = 2	6	353.7 (M:353.7)	1.76	4	116.9
HXK1_MOUSE	Hexokinase-1 OS = Mus musculus GN = Hk1 PE = 1 SV = 3	2	120.5 (M:120.5)	1.76	1	
CISY_MOUSE	Citrate synthase, mitochondrial OS = Mus musculus GN = Cs PE = 1 SV = 1	6	283.3 (M:283.3)	1.77	3	108.37
TTBK1_MOUSE	Tau-tubulin kinase 1 OS = Mus musculus GN = Ttbk1 PE = 2 SV = 3	1	34.1 (M:34.1)	1.77	1	
FOXP3_MOUSE	Forkhead box protein P3 OS = Mus musculus GN = Foxp3 PE = 1 SV = 1	1	25.1 (M:25.1)	1.77	1	
RS7_MOUSE	40S ribosomal protein S7 OS = Mus musculus GN = Rps7 PE = 2 SV = 1	2	65.6 (M:65.6)	1.78	1	
PPR26_MOUSE	Protein phosphatase 1 regulatory subunit 26 OS = Mus musculus GN = Ppp1r26 PE = 2 SV = 2	1	27.4 (M:27.4)	1.81	1	
CDC42_MOUSE	Cell division control protein 42 homolog OS = Mus musculus GN = Cdc42 PE = 1 SV = 2	3	146.6 (M:146.6)	1.83	1	
KPCB_MOUSE	Protein kinase C beta type OS = Mus musculus GN = Prkcb PE = 1 SV = 4	1	66.4 (M:66.4)	1.84	1	
GCAB_MOUSE	Ig gamma-2A chain C region secreted form OS = Mus musculus PE = 1 SV = 1	2	82.0 (M:82.0)	1.88	1	
NP1L1_MOUSE	Nucleosome assembly protein 1-like 1 OS = Mus musculus GN = Nap1l1 PE = 1 SV = 2	1	29.8 (M:29.8)	1.89	1	
ORN_MOUSE	Oligoribonuclease, mitochondrial OS = Mus musculus GN = Rexo2 PE = 1 SV = 2	1	57.6 (M:57.6)	1.91	1	
FBX41_MOUSE	F-box only protein 41 OS = Mus musculus GN = Fbxo41 PE = 1 SV = 3	1	36.8 (M:36.8)	1.97	1	
PPR3B_MOUSE	Protein phosphatase 1 regulatory subunit 3B OS = Mus musculus GN = Ppp1r3b PE = 1 SV = 1	1	29.8 (M:29.8)	1.97	1	

(*continued on next page*)

Table 1 (*continued*)

Accession	Protein	Identified numbers	Scores	OVX/ Control	Quantified peptides	CV (%)
ANKL2_MOUSE	Ankyrin repeat and LEM domain-containing protein 2 OS = Mus musculus GN = Ankle2 PE = 2 SV = 2	1	28.0 (M:28.0)	1.98	1	
UD17 C_MOUSE	UDP-glucuronosyltransferase 1-7C OS = Mus musculus GN = Ugt1a7c PE = 2 SV = 1	1	80.4 (M:80.4)	1.99	1	
LMOD1_MOUSE	Leiomodin-1 OS = Mus musculus GN = Lmod1 PE = 2 SV = 1	2	73.5 (M:73.5)	2.07	1	
ETFA_MOUSE	Electron transfer flavoprotein subunit alpha, mitochondrial OS = Mus musculus GN = Etfa PE = 1 SV = 2	4	164.7 (M:164.7)	2.13	4	174.79
A1AT4_MOUSE	Alpha-1-antitrypsin 1-4 OS = Mus musculus GN = Serpina1d PE = 2 SV = 1	5	304.6 (M:304.6)	2.2	2	75.82
SRRM2_MOUSE	Serine/arginine repetitive matrix protein 2 OS = Mus musculus GN = Srrm2 PE = 1 SV = 3	1	42.7 (M:42.7)	2.29	1	
PDXK_MOUSE	Pyridoxal kinase OS = Mus musculus GN = Pdxk PE = 1 SV = 1	1	54.2 (M:54.2)	2.31	1	
CK016_MOUSE	Uncharacterized protein C11orf16 homolog OS = Mus musculus GN = D7h11orf16 PE = 2 SV = 2	1	32.6 (M:32.6)	2.4	1	
MERL_MOUSE	Merlin OS = Mus musculus GN = Nf2 PE = 1 SV = 2	1	35.5 (M:35.5)	2.4	1	
IMB1_MOUSE	Importin subunit beta-1 OS = Mus musculus GN = Kpnb1 PE = 1 SV = 2	1	31.7 (M:31.7)	2.43	1	
MFAP4_MOUSE	Microfibril-associated glycoprotein 4 OS = Mus musculus GN = Mfap4 PE = 1 SV = 1	2	139.7 (M:139.7)	2.6	2	53.07
MYO1C_MOUSE	Unconventional myosin-Ic OS = Mus musculus GN = Myo1c PE = 1 SV = 2	1	79.8 (M:79.8)	2.77	1	
RSU1_MOUSE	Ras suppressor protein 1 OS = Mus musculus GN = Rsu1 PE = 2 SV = 3	5	261.6 (M:261.6)	2.94	3	203.09
ATP5I_MOUSE	ATP synthase subunit e, mitochondrial OS = Mus musculus GN = Atp5i PE = 1 SV = 2	1	30.2 (M:30.2)	3.03	1	
DLDH_MOUSE	Dihydrolipoyl dehydrogenase, mitochondrial OS = Mus musculus GN = Dld PE = 1 SV = 2	2	104.7 (M:104.7)	4.28	1	
VAT1_MOUSE	Synaptic vesicle membrane protein VAT-1 homolog OS = Mus musculus GN = Vat1 PE = 1 SV = 3	1	81.9 (M:81.9)	6.15	1	
SPR1A_MOUSE	Cornifin-A OS = Mus musculus GN = Sprr1a PE = 2 SV = 1	5	233.9 (M:233.9)	6.41	1	
S10AA_MOUSE	Protein S100-A10 OS = Mus musculus GN = S100a10 PE = 2 SV = 2	1	48.9 (M:48.9)	8.42	1	
HS3SB_MOUSE	Heparan sulfate glucosamine 3-O-sulfotransferase 3B1 OS = Mus musculus GN = Hs3st3b1 PE = 2 SV = 2	1	33.9 (M:33.9)	23.13	1	

ATP = adenosine triphosphate; ANK = ankyrin; CV = coefficient of variation; GN = gene name; NADH = nicotinamide adenine dinucleotide; NADP = nicotinamide adenine dinucleotide phosphate; OS = organism species; OVX = ovariectomy; PE= protein existence; PH = pleckstrin homology; SV = sequence version; WD = tryptophan-aspartic acid.

[a] As most proteins were identi fied and quantified with one peptide, which do not have CV (%), possibly due to their less abundance in tissue; these protein ratios could be reliable.

IHC staining to determine ZO-2 protein locations (Fig. 3A). The IHC analyses show that ZO-2 was mainly expressed on the urothelium. Western blot analysis revealed that ZO-2 expression was significantly lower ($p < 0.01$) in the bladder of OVX-treated mice than in the control group. By contrast, the ZO-2 expression was significantly increased ($p < 0.05$) in the bladder in the OVX + E2 group than in the OVX group (Fig. 3B).

Discussion

In the present study, we found that urothelial thickness significantly decreased in the bladder of OVX mice, although the apparent damage of the urothelium does not lead to typical signs of a leaky barrier such as edema or inflammation. These findings suggest that the damage of the urothelium might lead to typical signs of a leaky barrier, which might result in urinary frequency in OVX mice.

Table 2
In terms of Gene Ontology database, the differentially expressed proteins of bladder from OVX mice were divided into biological process.

	Networks
1	Cytoskeleton: actin filaments
2	Cytoskeleton: regulation of cytoskeleton rearrangement
3	Muscle contraction
4	Cell adhesion: integrin-mediated cell-matrix adhesion
5	Development: skeletal muscle development
6	Signal transduction: neuropeptide signaling pathways
7	Immune response: phagosome in antigen presentation
8	Cell adhesion: platelet aggregation
9	Cytoskeleton: intermediate filaments
10	Immune response: phagocytosis

This is the first study that estimated the changes in bladder protein expression related to OVX-induced OAB. We found 73 differentially expressed proteins between OVX-treated and control female mice. The expression of ZO-2, a tight junction protein, was affected the most by OVX. Urothelial tight junctions play an important role in the formation of the blood–urine barrier. Tight junctions are essential for normal function of epithelia, restricting paracellular diffusion and contributing to the maintenance of cell surface polarity. Superficial cells of the urothelium develop tight junctions, the basis for the paracellular permeability barrier of the bladder against diffusion of urinary solutes. Tight junctions-associated ZO proteins were localized at cell margins [13], damages to urothelial tight junctions disrupt barrier function, which induces urinary tract diseases [14]. In the present study, we found that the protein level of ZO-2, a scaffolding tight junction protein, decreased in the bladder of OVX mice. These findings suggest that scaffold proteins such as ZO-2 may be sensitive to estrogen deficiency. A possible future study regarding a ZO-2 knockout mouse [30,31] which might express the OAB trait even without OVX. Moreover, our results could highlight potential drug targets in urothelial injury [32], including defects in the urothelial barrier and disruption in tight junction integrity, which could be a therapeutic strategy for OAB.

In this study, ZO-2 expression in the bladder was significantly increased in the OVX + E2 group, indicating increased expression of the tight junction in the urothelium of the bladder. Our data suggest that increased synthesis of these tight junction proteins can be attributed to activation by E2. Urothelial thickness in the bladder was increased in the OVX + E2 group, and voiding interval values were significantly increased in the OVX + E2 group. There is evidence that these tight junction proteins, urothelium, and E2 may play important roles in OAB.

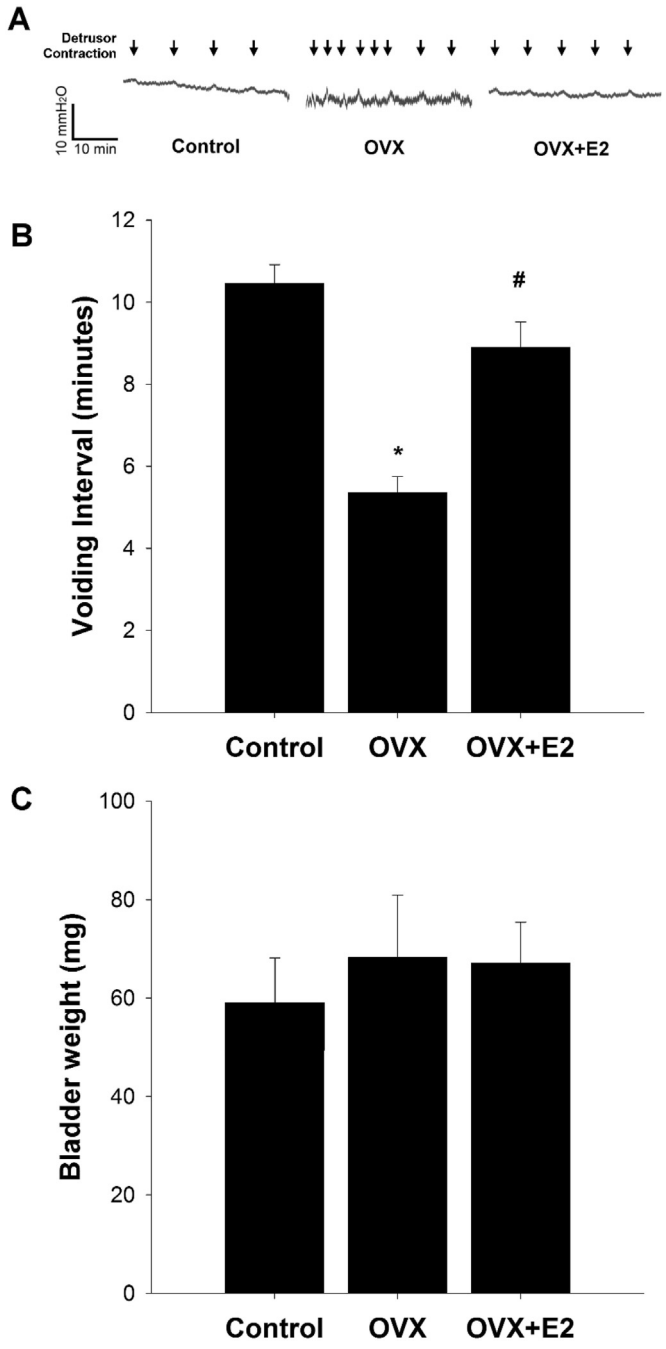

Figure 1. Voiding interval values in the different groups. (A and B) Cystometry traces between control, OVX-induced OAB, and OVX + E2 group in female mice; (C) bladder weights in the different groups. Each bar represents the mean ± standard deviation of six individual mice. * Significantly different from the values in the sham control ($p < 0.05$). ** Significantly different from the values in the OVX control ($p < 0.05$). E2 = estradiol; OVX = ovariectomy.

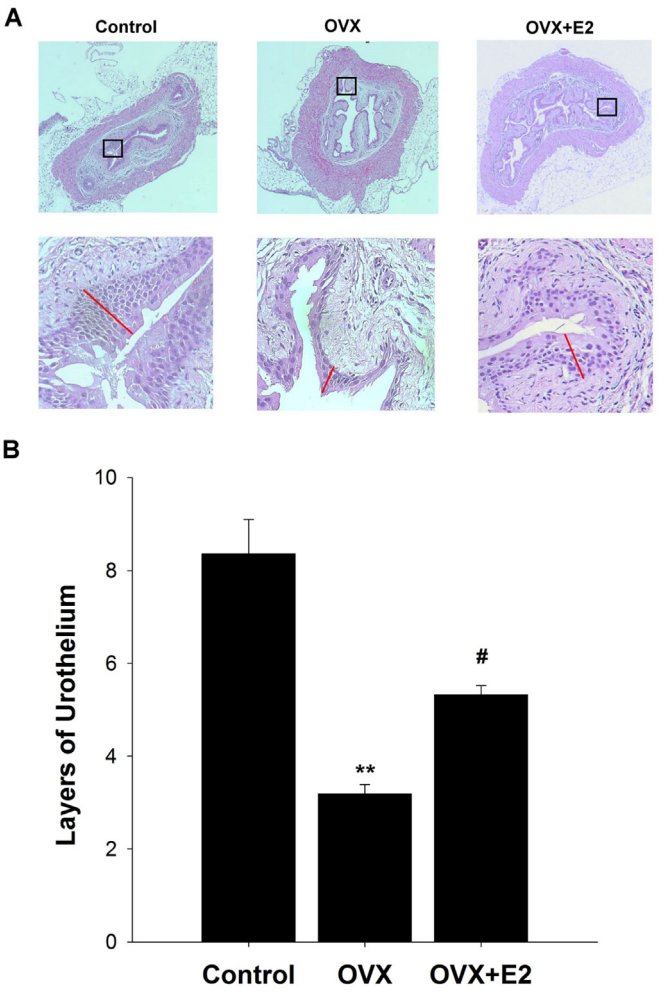

Figure 2. (A) Histological examination in bladder by hematoxylin and eosin (H&E) stain between control, OVX-induced OAB, and OVX + E2 groups in female mice; (B) average thickness of urothelium, lamina propria and submucosa, and muscularis in the different groups. The mice were sacrificed, and the bladders were harvested for H&E stain. Cross sections of the specimens were examined; the mean thickness of the four regions of the urothelium near the two diagonal lines in the transverse sections of the midbladder was evaluated. Each bar represents the mean ± standard deviation of six individual mice. * Significantly different from the values in the normal control ($p < 0.01$). ** Significantly different from the values in the OVX control ($p < 0.05$). E2 = estradiol; H&E = hematoxylin and eosin; OAB = overactive bladder; OVX = ovariectomy.

Our study has certain limitations: (1) the pelvic floor structure of the mouse, which is a quadruped and has a lax abdominal wall, is different from that of a human female [33]. Therefore, the results of this study need to be carefully applied to humans; (2) urodynamic studies were conducted under anaesthesia [34]; (3) because a large protein profile was established in the proteomic study, we could not confirm all identified proteins by Western blot [35]; and (4) more studies to evaluate other important urothelial tight junction proteins of the superficial layer, how urothelial barrier is compromised, and how the changes of ZO-2 may be related to reduced voiding intervals are warranted for further clarity.

In protein sample preparation for proteomics, the same absolute protein quantity in control and OVX samples were obtained and compared. Therefore, the proteins with fold changes were compared on the basis of the same total protein amounts in control and OVX bladder samples. In addition to the proteomic analysis, we used immunohistochemistry staining to verify the location of ZO2 expression and used Western blot to confirm protein expression level with the loading/internal control GAPDH. These comparison methods might exclude the possible concern of protein changes due to less urothelium. Nevertheless, the differences in protein expression may likely have more to do with loss of epithelial tissue in the bladder than with actual changes in expression at the mRNA and protein level.

Our results suggest that OVX can induce OAB in female mice. E2 supplementation in OVX mice can rescue OAB. E2-mediated increase in bladder function in OVX mice involves overexpression of

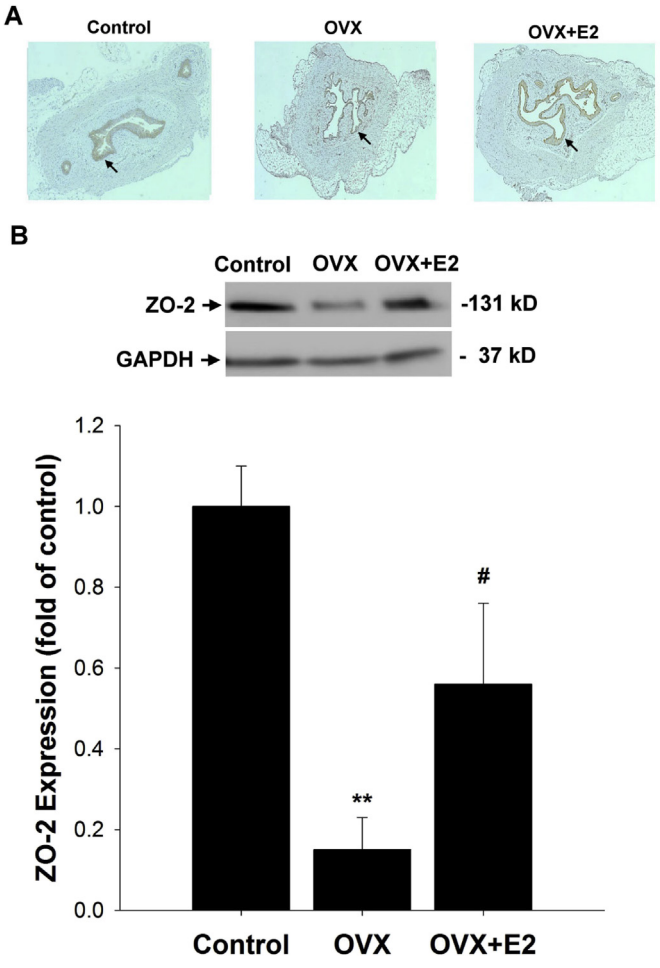

Figure 3. Location and alterations of tight junction protein ZO-2 (zonula occludens-2, ZO-2) expression in bladder as indicated by (A) IHC staining; (B) Western blot analyses, respectively, between control, OVX-induced OAB, and OVX + E2 groups in female mice. The bladder was histologically examined with IHC staining for indicating the ZO-2 protein expression (brown, positive staining, arrows) regions of the bladder urothelium. The sections were then incubated with the primary antibody derived from rabbit (anti-ZO-2 antibody). Western blot analysis was performed with the use of the same antibody. The intensity of each band (GAPDH was used as loading control for normalization) was quantified using a densitometer. The values are calculated by fold and expressed as mean ± standard deviation of six individual mice. * Significantly different from the values in the normal control ($p < 0.01$). ** Significantly different from the values in the OVX control ($p < 0.05$). E2 = estradiol; GAPDH = glyceraldehyde 3-phosphate dehydrogenase; IHC = immunohistochemistry; OAB = overactive bladder; OVX = ovariectomy; ZO-2 = zonula occludens-2

ZO-2 and protection of urothelial integrity in the bladder suggesting an important role of urothelial tight junctions in OAB. This study has shown that the bladder actively undergoes multiple biological processes in response to OVX and OVX with E2 stimuli. These changes could be related to the protein expression profile involved in OAB and will therefore be useful to highlight potential clinical drug targets in the future.

Conflicts of interest

The authors have no conflicts of interest relevant to this article.

Acknowledgments

This work was supported in part by Taiwan Ministry of Science and Technology (NSC101-2314-B-039-018 and MOST104-2320-B-039-016-MY3), China Medical University Hospital (DMR-105-063), CMU under the Aim for Top University Plan of the Taiwan Ministry of Education, and Taiwan Ministry of Health and Welfare Clinical Trial and Research Center of Excellence (MOHW105-TDU-B-212-133019). HYC and CJC contributed equally to this study.

References

[1] Bozkurt M, Yumru AE, Sahin L. Pelvic floor dysfunction, and effects of pregnancy and mode of delivery on pelvic floor. Taiwan J Obstet Gynecol 2014;53:452–8.
[2] Tsai CP, Cheng KL, Liu CK, Chou MM, Chen GD, Hung MJ. The coexistence of interstitial cystitis and overactive bladder in a patient with lower urinary tract symptoms. Taiwan J Obstet Gynecol 2014;53:263–6.
[3] Wang CL, Wu CH, Liu CM, Shen CJ, Lin KL, Long CY. Clinical and urodynamic effects of tolterodine in women with an overactive bladder. Taiwan J Obstet Gynecol 2013;52:381–4.
[4] Liang CC, Chang YL, Lin YH, Chang SD. Significance of bladder trabeculation in postmenopausal women with severe pelvic organ prolapse: clinical and urodynamic assessments. Menopause 2013;20:813–7.
[5] Liang CC, Tseng LH, Chang YL, Chang SD. Predictors of persistence of preoperative urgency incontinence in women following pelvic organ prolapse repair. Taiwan J Obstet Gynecol 2015;54:682–5.
[6] Irwin DE, Milsom I, Hunskaar S, Reilly K, Kopp Z, Herschorn S, et al. Population-based survey of urinary incontinence, overactive bladder, and other lower urinary tract symptoms in five countries: results of the EPIC study. Eur Urol 2006;50:1306–14. discussion 14–5.
[7] Wu IC, Lin CC, Hsiung CA. Emerging roles of frailty and inflammaging in risk assessment of age-related chronic diseases in older adults: the intersection between aging biology and personalized medicine. Biomedicine (Taipei) 2015;5:1.
[8] Hashim H, Abrams P. Drug treatment of overactive bladder: efficacy, cost, and quality-of-life considerations. Drugs 2004;64:1643–56.
[9] Andersson KE, Fullhase C, Soler R. Urothelial effects of oral agents for overactive bladder. Curr Urol Rep 2008;9:459–64.
[10] Nocchi L, Daly DM, Chapple C, Grundy D. Induction of oxidative stress causes functional alterations in mouse urothelium via a TRPM8-mediated mechanism: implications for aging. Aging Cell 2014;13:540–50.
[11] Daly DM, Nocchi L, Liaskos M, McKay NG, Chapple C, Grundy D. Age-related changes in afferent pathways and urothelial function in the male mouse bladder. J Physiol 2014;592:537–49.
[12] Dozmorov M, Stone 2nd R, Clifford JL, Sabichi AL, Engles CD, Hauser PJ, et al. System level changes in gene expression in maturing bladder mucosa. J Urol 2011;185:1952–8.
[13] Rickard A, Dorokhov N, Ryerse J, Klumpp DJ, McHowat J. Characterization of tight junction proteins in cultured human urothelial cells. In vitro Cell Dev Biol Anim 2008;44:261–7.
[14] Kreft ME, Hudoklin S, Jezernik K, Romih R. Formation and maintenance of blood–urine barrier in urothelium. Protoplasma 2010;246:3–14.
[15] Lee KC. Changes of muscarinic receptors and connexin-43 expression as a mechanism of overactive bladder in ovariectomized rats. World J Urol 2015;33:1875–9.
[16] Blakeman PJ, Hilton P, Bulmer JN. Oestrogen and progesterone receptor expression in the female lower urinary tract, with reference to oestrogen status. BJU Int 2000;86:32–8.
[17] Sturdee DW, Pines A. International Menopause Society Writing Group, Archer DF, Baber RJ, Barlow D, et al. Updated IMS recommendations on postmenopausal hormone therapy and preventive strategies for midlife health. Climacteric 2011;14:302–20.
[18] Demaagd GA, Davenport TC. Management of urinary incontinence. P T 2012;37:345–361H.
[19] Tomaszewski J. Postmenopausal overactive bladder. Prz Menopauzalny 2014;13:313–29.
[20] Hammack BN, Fung KY, Hunsucker SW, Duncan MW, Burgoon MP, Owens GP, et al. Proteomic analysis of multiple sclerosis cerebrospinal fluid. Mult Scler 2004;10:245–60.
[21] Chen HY, Chen WC, Lin YN, Chen YH. Synergistic effect of vaginal trauma and ovariectomy in a murine model of stress urinary incontinence: upregulation of urethral nitric oxide synthases and estrogen receptors. Mediators Inflamm 2014;2014:314846.
[22] Chen HY, Chen CJ, Lin YN, Chen YH, Chen WC, Chen CM. Proteomic analysis related to stress urinary incontinence following vaginal trauma in female mice. Eur J Obstet Gynecol Reprod Biol 2013;171:171–9.
[23] Chen HY, Lin YN, Chen YH, Chen WC. Stress urinary incontinence following vaginal trauma involves remodeling of urethral connective tissue in female mice. Eur J Obstet Gynecol Reprod Biol 2012;163:224–9.
[24] Tsai JJ, Lin HJ. Clinical manifestations and management of buried bumper syndrome in patients with percutaneous endoscopic gastrostomy. Gastrointest Endosc 2008;68:580–4.
[25] Lin YH, Liu G, Daneshgari F. A mouse model of simulated birth trauma induced stress urinary incontinence. Neurourol Urodyn 2008;27:353–8.
[26] Boudes M, Uvin P, Kerselaers S, Vennekens R, Voets T, De Ridder D. Functional characterization of a chronic cyclophosphamide-induced overactive bladder model in mice. Neurourol Urodyn 2011;30:1659–65.

[27] Tsai JR, Wang HM, Liu PL, Chen YH, Yang MC, Chou SH, et al. High expression of heme oxygenase-1 is associated with tumor invasiveness and poor clinical outcome in nonsmall cell lung cancer patients. Cell Oncol (Dordr) 2012;35:461–71.
[28] Lin SY, Hsu WH, Lin CC, Chen CJ. Mass spectrometry-based proteomics in chest medicine, gerontology, and nephrology: subgroups omics for personalized medicine. Biomedicine (Taipei) 2014;4:25.
[29] Liu HH, Tsai YS, Lai CL, Tang CH, Lai CH, Wu HC, et al. Evolving personalized therapy for castration-resistant prostate cancer. Biomedicine (Taipei) 2014;4:2.
[30] Phua DC, Xu J, Ali SM, Boey A, Gounko NV, Hunziker W. ZO-1 and ZO-2 are required for extraembryonic endoderm integrity, primitive ectoderm survival and normal cavitation in embryoid bodies derived from mouse embryonic stem cells. PLoS One 2014;9:e99532.
[31] Xu J, Anuar F, Ali SM, Ng MY, Phua DC, Hunziker W. Zona occludens-2 is critical for blood-testis barrier integrity and male fertility. Mol Biol Cell 2009;20:4268–77.
[32] Liao WL, Tsai FJ. Personalized medicine: a paradigm shift in healthcare. BioMedicine 2013;3:66–72.
[33] Fujimura M, Izumimoto N, Momen S, Yoshikawa S, Kobayashi R, Kanie S, et al. Characteristics of TRK-130 (Naltalimide), a novel opioid ligand, as a new therapeutic agent for overactive bladder. J Pharmacol Exp Ther 2014;350:543–51.
[34] Schneider MP, Hughes Jr FM, Engmann AK, Purves JT, Kasper H, Tedaldi M, et al. A novel urodynamic model for lower urinary tract assessment in awake rats. BJU Int 2015;115(Suppl 6):8–15.
[35] Didangelos A, Stegemann C, Mayr M. The -omics era: proteomics and lipidomics in vascular research. Atherosclerosis 2012;221:12–7.